NeuroImage: Clinical 37 (2023) 103311

Contents lists available at ScienceDirect

NeuroImage: Clinical

journal homepage: www.elsevier.com/locate/ynicl

Lesion location across diagnostic regions in multiple sclerosis

Viola Pongratz [a,*], Matthias Bussas [a], Paul Schmidt [b], Sophia Grahl [a], Christiane Gasperi [a], Malek El Husseini [c], Laura Harabacz [a], Viktor Pineker [c], Dominik Sepp [c], Lioba Grundl [c], Benedikt Wiestler [c], Jan Kirschke [c], Claus Zimmer [c], Achim Berthele [a], Bernhard Hemmer [a,d], Mark Mühlau [a]

[a] Neurology, Technische Universität München, Ismaninger Str. 22, Munich 81541, Germany
[b] Paul Schmidt, Statistical Consulting, Große Seestraße 8, Berlin 13086, Germany
[c] Neuroradiology, Technische Universität München, Ismaninger Str. 22, Munich 81541, Germany
[d] Munich Cluster for Systems Neurology (SyNergy), Feodor-Lynen-Str. 17, Munich 81377, Germany

ARTICLE INFO

Keywords:
Multiple sclerosis
Demyelinating diseases
Magnetic resonance imaging
White matter lesion

ABSTRACT

Background: Lesions in the periventricular, (juxta)cortical, and infratentorial region, as visible on brain MRI, are part of the diagnostic criteria for Multiple sclerosis (MS) whereas lesions in the subcortical region are currently only a marker of disease activity. It is unknown whether MS lesions follow individual spatial patterns or whether they occur in a random manner across diagnostic regions.
Aim: First, to describe cross-sectionally the spatial lesion patterns in patients with MS. Second, to investigate the spatial association of new lesions and lesions at baseline across diagnostic regions.
Methods: Experienced neuroradiologists analyzed brain MRI (3D, 3T) in a cohort of 330 early MS patients. Lesions at baseline and new solitary lesions after two years were segmented (manually and by consensus) and classified as periventricular, (juxta)cortical, or infratentorial (diagnostic regions) or subcortical—with or without Gadolinium-enhancement. Gadolinium enhancement of lesions in the different regions was compared by Chi square test. New lesions in the four regions served as dependent variable in four zero-inflated Poisson models each with the six independent variables of lesions in the four regions at baseline, age and gender.
Results: At baseline, lesions were most often observed in the subcortical region (mean 13.0 lesions/patient), while lesion volume was highest in the periventricular region (mean 2287 μl/patient). Subcortical lesions were less likely to show gadolinium enhancement (3.1 %) than juxtacortical (4.3 %), periventricular (5.3 %) or infratentorial lesions (7.2 %). Age was inversely correlated with new periventricular, juxtacortical and subcortical lesions. New lesions in the periventricular, juxtacortical and infratentorial region showed a significant autocorrelative behavior being positively related to the number of lesions in the respective regions at baseline. New lesions in the subcortical region showed a different behavior with a positive association with baseline periventricular lesions and a negative association with baseline infratentorial lesions.
Conclusion: Across regions, new lesions do not occur randomly; instead, new lesions in the periventricular, juxtacortical and infratentorial diagnostic region are associated with that at baseline. Lesions in the subcortical regions are more closely related to periventricular lesions. Moreover, subcortical lesions substantially contribute to lesion burden in MS but are less likely to show gadolinium enhancement (than lesions in the diagnostic regions).

1. Introduction

The diagnosis of multiple sclerosis (MS) is based on typical neurological symptoms, the presence of lesions in the central nervous system, and their dissemination in space and time. Since the introduction of the McDonald criteria in 2001 (McDonald et al., 2001), magnetic resonance imaging (MRI) can be used to demonstrate dissemination in space and time. In the current revised version of McDonald criteria (Thompson et al., 2018), dissemination in space as demonstrated by MRI is fulfilled by at least one lesion in two or more typical regions: periventricular,

* Corresponding author at: Technical University of Munich, School of Medicine, Department of Neurology, Ismaningerstr. 22, Munich D-81675, Germany.
E-mail address: viola.biberacher@tum.de (V. Pongratz).

https://doi.org/10.1016/j.nicl.2022.103311
Received 9 June 2022; Received in revised form 3 December 2022; Accepted 30 December 2022
Available online 5 January 2023

(juxta)cortical, and infratentorial brain regions, and the spinal cord. Dissemination in time can be demonstrated by MRI by the simultaneous presence of gadolinium-enhancing and non-enhancing lesions or by a new lesion in any brain region or the spinal cord on a follow-up MRI. Subcortical lesions are located in the supratentorial white matter without touching the ventricles or the cortical ribbon. Subcortical lesions are also a common finding in MS patients. In patients with clinically isolated syndrome, lesions clusters in white matter tracts in the subcortical area have been shown to predict conversion to relapsing remitting multiple sclerosis, as did lesion clusters in the diagnostic regions (Giorgio et al., 2013). However, subcortical lesions are not part of the diagnostic criteria to demonstrate dissemination in space as they are also found in normal aging (Awad et al., 1986; Hunt et al., 1989; King et al., 2014; Scharf et al., 2019), and patients with other neurological disease such as migraine (Lapucci et al., 2019), or cerebral small vessel disease (Geraldes et al., 2018). Yet a new subcortical lesion in a follow-up MRI of a patient with clinically isolated syndrome demonstrates dissemination in time according to the diagnostic criteria and has also been interpreted as active disease in pivotal clinical trials (Cohen et al., 2016; Cohen et al., 2012; Coles et al., 2012; Comi et al., 2001; Comi et al., 2009; Ebers, 1998; Fox et al., 2012; Giovannoni et al., 2010; Gold et al., 2012; Hauser et al., 2020; Hauser et al., 2017; Kappos, 1998; Kappos et al., 2018; Kappos et al., 2021; Kappos et al., 2010; Khatri et al., 2011; Leist et al., 2014; Montalban et al., 2016; Polman et al., 2006).

MS lesions preferentially occur around small veins, which explains the predilection sites around subependymal veins for periventricular lesions, around superficial veins for (juxta)cortical lesions and around deep brainstem veins for infratentorial lesions (Absinta et al., 2016; Tallantyre et al., 2008). However, other mechanisms than venous anatomy may contribute to lesion location, and it is unknown whether MS lesions follow individual spatial patterns or whether they occur in a random manner across regions. To the best of our knowledge, we are only aware of one study that found positive correlations between baseline lesion locations and new lesion location, especially in the supratentorial brain (Gaetano et al., 2020). In this work, we studied the spatial distribution of brain lesions in MS cross-sectionally and longitudinally. We also tested for differences in gadolinium-enhancement and for association with age.

2. Materials and methods

2.1. Subjects and study design

This study was performed in accordance with the Code of Ethics of the World Medical Association (Declaration of Helsinki) for experiments involving humans and was approved by the local ethics committee. Written informed consent was obtained from all patients. We retrospectively analyzed data that were collected in an observational study (TUM-MS) at the Department of Neurology at the Technical University of Munich between August 2008 and August 2017. Inclusion criteria were a diagnosis of clinically isolated syndrome or MS according to current diagnostic criteria (Thompson et al., 2018). We included all patients that had received a baseline brain MRI scan and a follow-up scan after 1.5 to 2.5 years.

Intravenous corticosteroids were administered in 49 patients within 30 days prior to the baseline brain MRI scan and in 8 patients within 30 days prior to the follow-up brain MRI scan. Inclusion of patients with previous corticosteroid treatment was justified for our study purpose as we focused on lesion count which should not be influenced by corticosteroid treatment.

Disability was determined by Expanded Disability Status Scale (EDSS) by the treating neurologist. Patient characteristics are summarized in Table 1.

Table 1
Patient characteristicsTables.

Patient characteristics		
Sex (male; female)	114; 216	
	baseline	follow-up
Age (years; mean ± SD; range)	38.5 ± 9.7; 19–65	40.5 ± 9.8; 21–67
Disease duration (years; mean ± SD; range)	1.6 ± 3.3; 0–21.2	3.7 ± 3.3; 1.6 – 23.6
Disease course (CIS; RRMS; SPMS)	25; 305; 0	7; 321; 2
Disease modifying drugs	none 280; DMF 3; GA 12; IFN 32; NTZ 2, study medication 1	none 83; DMF 27 FTY 14; GA 68; IFN 114; NTZ 20, TFN 2; RTX 1; study medication 1
EDSS (N; median; range)	284; 1.5; 0–6.0	321; 1.5; 0–6.5

CIS, clinically isolated syndrome; DMF, dimethyl fumarate; EDSS, Expanded Disability Status Scale; FTY, fingolimod; GA, glatiramer acetate; IFN, beta interferon; NTZ, natalizumab; RRMS, relapsing remitting multiple sclerosis; RTX, rituximab; SD, standard deviation; SPMS, secondary progressive multiple sclerosis; TFN, teriflunomide.

2.2. Magnetic resonance imaging

2.2.1. Scanning protocol

All brain images were acquired on the same 3T scanner (Achieva, Philips, Netherlands). The scanning protocol included 3D GRE T1-weighted sequence before and after gadolinium injection (orientation, 170 contiguous sagittal 1 mm slices; field of view, 240×240 mm; voxel size, 1.0×1.0×1.0 mm; repetition time (TR), 9 ms; echo time (TE), 4 ms), and 3D FLAIR sequence (orientation, 144 contiguous axial 1.5 mm slices; field of view, 230×185 mm; voxel size, 1.0×1.0×1.5 mm; TR, 10 000 ms; TE, 140 ms; inversion time, 2750 ms).

2.2.2. T2-hyperintense white matter lesion segmentation

Brain T2-hyperintense white matter lesions were segmented by the software LST (lesion segmentation tool, https://www.applied-statistics.de/lst) and manually corrected by a group of experienced neuroradiologists. Each brain MRI scan was first independently segmented by two neuroradiologists. In a second step, the two independent readers reached a consensus segmentation. Lesions were classified as periventricular, (juxta)cortical or infratentorial according to current diagnostic criteria (Thompson et al., 2018): Periventricular lesions directly abut the ventricles, (juxta)cortical lesions directly abut the cortical ribbon, whereas infratentorial lesions are located anywhere in the brainstem, cerebellum or cerebellar peduncles. Supratentorial white matter lesions, neither directly abutting the ventricles nor the cortical ribbon, were classified as subcortical lesions. If two lesions abutted each other but were clearly distinguishable as two lesions, they were counted as 2 separate lesions. If lesions were part of a larger confluent lesion which did not allow the identification of the underlying individual lesions, this confluent lesion was counted as one lesion. For the follow-up image, only new or enlarging lesions were segmented. Details on the method for segmentation of new or enlarging lesions have been described in previous studies (Eichinger et al., 2019; Eichinger et al., 2017). First, baseline and follow-up images were read side by side and analyzed for new and enlarging lesions by using FLAIR-based subtraction maps together with the respective source images. Areas of high signal intensity on these subtraction images were classified as new and enlarging lesions if they were not present at baseline MRI and if they could be verified on the nonprocessed source images. New and enlarging lesions were marked with open-source software ITK-SNAP version 3.6 (Yushkevich et al., 2006). During the revision process, a separate analysis of new solitary and new enlarging lesions was conducted. Therefore, lesion

changes abutting at least one voxel of another lesion in the baseline image were classified as enlarging lesions. All other lesion changes were classified as new solitary lesions. This definition implies that new but confluent lesions are counted as enlarging lesions. Visual inspection revealed that the majority of the identified "enlarging" lesions were new but confluent lesions. The differentiation between new and enlarging lesions was not possible in one patient. Further statistical analyses were performed with new solitary lesions only, enlarging and new but confluent lesions were dropped out.

In a second readout, baseline and follow-up images were assessed for contrast-enhancing lesions. For this analysis, we used the T1-weighted images obtained before and after contrast material administration and the corresponding subtraction images obtained with the T1-weighted sequences.

2.3. Statistical analysis

IBM SPSS Statistics version 29 and GNU R version 4.0.3 (R: A language and environment for statistical computing. R Foundation for Statistical Computing, Vienna, Austria. URL https://www.R-project.org/) were used to analyze and visualize data. Gadolinium enhancement of lesions in the different regions was compared pairwise by Chi square test in Excel (Microsoft Office 2013). For the following three tests, logarithmic transformation was performed for all lesion numbers and volumes: log 10 (lesion number +1).

- Paired T-tests for the assessment of differences in baseline and new lesion number and volume in the different brain regions.
- Pearson's correlation to evaluate the association between the number of new solitary lesions in the different regions and age.
- Pearson's correlation to assess the association of baseline and new solitary lesions with EDSS at baseline and follow-up.

Temporal consistency of white matter lesion patterns (i.e., lesion distribution across diagnostic regions) was analyzed by independent zero-inflated Poisson (ZIP) models with numbers of new solitary lesions in the different regions as dependent variables, and baseline lesions in these regions as independent variables. We also corrected for age (continuous variable) and gender (factor). This specification was also used for the zero-inflated part of the model. Each ZIP model consists of two parts, one for modelling the risk of no new lesion (zero-inflated part) and one for modelling the number of new lesions (Poisson part). Therefore, a positive correlation of baseline lesions with new lesions can be demonstrated by a positive correlation with the number of lesions (more new lesions go along with more lesions at baseline) or by a negative correlation with the risk of no new lesion (more subjects with no new lesions than expected go along with less lesions at baseline). A negative correlation of baseline lesions with new lesions can be demonstrated by a negative correlation with the number of lesions or by a positive correlation with the risk of no new lesion. Results are presented as rate ratios for the Poisson part of the model and as odds ratios for the zero-inflated part. Negative correlations are indicated by values <1, positive correlations by values greater than 1. Model assumptions have been checked by residual diagnostics using simulation-based residuals as implemented in the R package DHARMa (https://www.rdocumentation.org/packages/DHARMa/versions/0.4.6, 2022). This included quantile-quantile plots (qq-plots) of residuals as well as diagnostic tests for over- and underdispersion and outliers. In all cases (models for PV lesions, SC lesions, JC lesions, and IT lesions), qq-plots showed no serious violations of the distributional assumption. Overdispersion was noted in the SC lesion and JC lesion models. Outliers were also identified for these models. This was expected as the maximum number of new lesions for these regions is 77 and 41, respectively. A sensitivity analysis excluding the 1 % highest response values was carried out to analyse the effect of outliers. Although no further outliers could be identified in these models and the overdispersion was reduced, the results of the coefficients changed only slightly. In order to address overdispersion in these regions negative binomial models with the same zero-inflated terms have been fitted. However, due to convergence problems, no direct comparison with the original models could be made. In summary, we could not find any convincing indication that the fitted models should not be used to assess the question at hand. Correction for multiple testing was performed by Benjamini-Hochberg procedure with a false discovery rate (FDR) level of 0.05 (Benjamini and Hochberg, 1995).

3. Results

3.1. Distribution of white matter lesions at baseline MRI

Number and volume of lesions in different regions at baseline are given in Table 2 and Fig. 1. Periventricular lesions were found in 92 %, subcortical lesions in 93 %, (juxta)cortical lesions in 79 % and infratentorial lesions in 52 % of all patients. Brain lesion volume was highest in the periventricular, followed by the subcortical, juxtacortical and infratentorial region. Brain lesion number was highest in the subcortical, followed by the periventricular, juxtacortial and infratentorial region. The differences in lesion number and volume in the different brain regions all were significant (all p-values < 0.001).

3.2. Gadolinium enhancement of lesions at baseline MRI

Gadolinium-enhancement was found in 5.3 % of periventricular lesions, 4.3 % of (juxta)cortical lesions, 3.1 % of subcortical lesions and 7.3 % of infratentorial lesions (Fig. 2). Differences in gadolinium enhancement between lesion numbers in different brain regions were significant (all p-values < 0.001) for all comparisons except between periventricular and (juxta)cortical lesions and between periventricular and infratentorial lesions.

3.3. Changes in lesion number and volume at follow-up MRI

Number and volumes of new lesions at the follow-up MRI are given in Table 3 and illustrated in Fig. 3. New solitary lesions were most often found in the subcortical region (mean 2.4), followed by the periventricular (mean 1.5), (juxta)cortical (mean 1.2) and infratentorial (mean

Table 2
Baseline MRI data.

	Number of patients	Mean ± SD	Range
Periventricular lesion number	330	6.5 ± 5.7	0–28
Periventricular lesion volume (µl)	330	2287.4 ± 5154.8	0–52131
Periventricular lesion size (µl)	305	330.4 ± 856.0	8.0 – 11,191
Juxtacortical lesion number	330	6.0 ± 12.6	0–123
Juxtacortical lesion volume (µl)	330	519.1 ± 1355.1	0–17998
Juxtacortical lesion size (µl)	260	123.1 ± 570.8	9.0 – 8999
Subcortical lesion number	330	13.0 ± 16.1	0–138
Subcortical lesion volume (µl)	330	652.1 ± 908.6	0–5613
Subcortical lesion size (µl)	307	53.1 ± 79.8	7.0 – 1272
Infratentorial lesion number	330	1.6 ± 2.6	0–20
Infratentorial lesion volume (µl)	330	149.7 ± 348.2	0–2962
Infratentorial lesion size (µl)	174	127.0 ± 294.2	8.0 – 2962
Periventricular Gd + lesion number	323	0.3 ± 1.0	0–10
Subcortical Gd + lesion number	323	0.4 ± 1.3	0–18
Juxtacortical Gd + lesion number	323	0.3 ± 0.9	0–8
Infratentorial Gd + lesion number	323	0.1 ± 0.4	0–3

GD, gadolinium; µl, microlitre; SD, standard deviation.

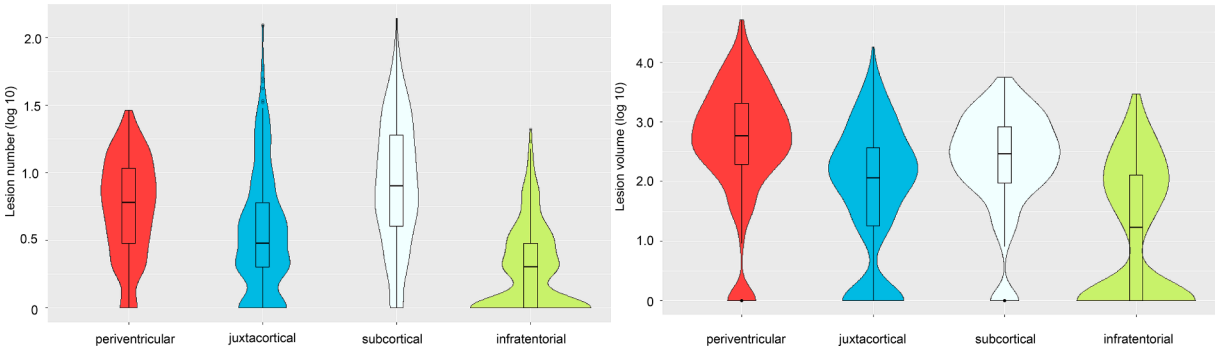

Fig. 1. Number (left panel) and volume (right panel) of lesions in the different regions at baseline are illustrated by violin plots with included boxplots. The y-axis is noted on a logarithmic scale.

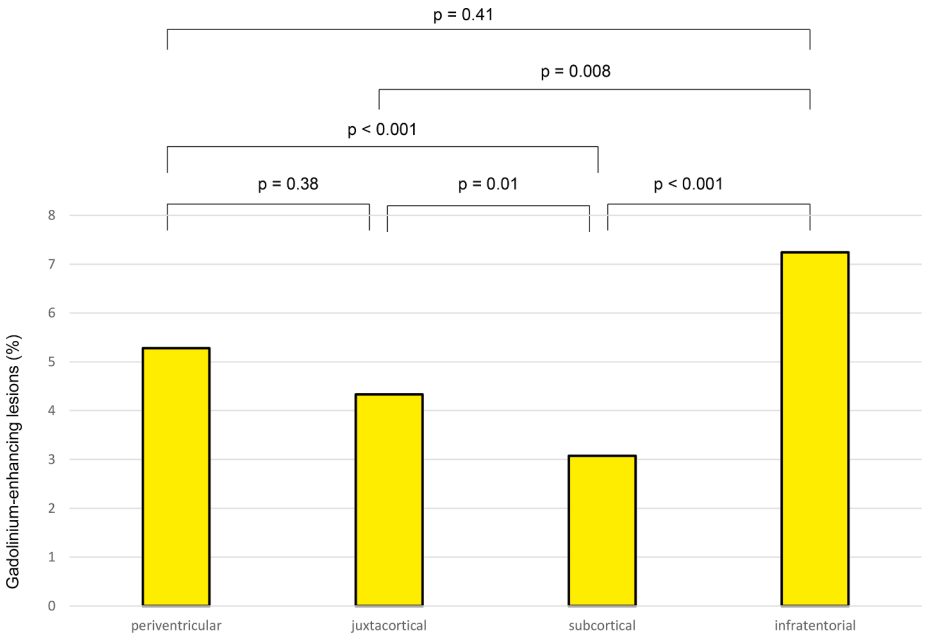

Fig. 2. The percentage of gadolinium enhancing lesions in each region is illustrated by bars for the group of patients with gadolinium-administration at the baseline MRI (N = 323). Significance derived from Chi square test comparisons of gadolinium enhancement in the different regions is indicated above the columns. Gd, gadolinium.

Table 3
Follow-up MRI data.

	New		Enlarging or new confluent	
	Lesion number (mean ± SD; range)	Lesion volume (mean ± SD; range)	Lesion number (mean ± SD; range)	Lesion volume (mean ± SD; range)
Periventricular lesions	1.5 ± 2.8; 0–28	372.9 ± 1062.4; 0 – 8689.0	0.46 ± 1.43; 0–13	258.4 ± 1152.9; 0 – 11940.0
Juxtacortical lesions	1.2 ± 3.5; 0–41	131.6 ± 592.5; 0 – 8599	0.09 ± 0.60; 0–9	31.9 ± 286.1; 0–3510
Subcortical lesions	2.4 ± 5.7; 0–77	214.7 ± 699.7; 0–10426	0.26 ± 1.05; 0–12	68.2 ± 373.4; 0–4819
Infratentorial lesions	0.3 ± 0.74; 0–7	33.8 ± 181.5; 0 – 2923	0.02 ± 0.13; 0–1	4.3 ± 45.2; 0–680

0.3) region. Highest increase in lesion volume was found in the periventricular region (mean 372.9 μl) followed by the subcortical (mean 214.7 μl), (juxta)cortical (mean 131.6 μl) and infratentorial (mean 33.8 μl) region. The difference between new periventricular and new subcortical log10-transformed lesion volume was not significant ($p = 0.9$). All other comparisons were significant (all p-values < 0.001).

New lesions (or parts of lesions) abutting another lesion in the baseline MRI scan (and therefore classified as enlarging or new confluent lesion) were most often found in the periventricular region, followed by the subcortical, juxtacortical and infratentorial region (Table 3). All comparisons were significant (enlarging/confluent juxtacortical versus infratentorial lesion number p 0.019, lesion volume p 0.045, all other p-values < 0.001). As enlarging lesions could not be further distinguished from new confluent lesions and per definition can only occur in the same region as the abutting lesion at baseline, further analyses were performed with new solitary lesions only.

3.4. Association of new solitary lesions with age

Age showed a negative correlation with the number of new solitary lesions in the periventricular, (juxta)cortical and subcortical region but not in the infratentorial region (periventricular $R = -0.238$, $p < 0.001$,

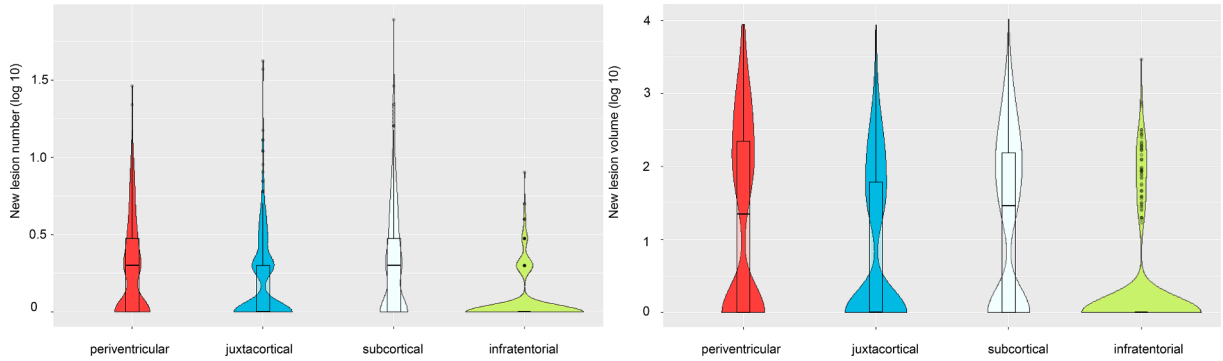

Fig. 3. Number (left panel) and volume (right panel) of new lesions in the different locations at follow-up MRI scan (N = 329) are illustrated by violin plots with included boxplots. The y-axis is noted on a logarithmic scale.

(juxta)cortical R = −0.135, p = 0.014, subcortical R = −0.172, p = 0.02, infratentorial R = −0.072, p = 0.19), meaning that younger patients show more new lesions (Fig. 4). Significant associations of new solitary lesions with age were confirmed in the ZIP models (Table 4).

3.5. Temporal association of lesion location across regions

The results of the ZIP models are illustrated in Fig. 5 and given in Table 4. The blue arrows indicate a positive association between baseline lesions and new solitary lesions (positive correlation with the number of lesions or negative correlation with the risk of no new lesion); red arrows indicate negative associations (negative correlation with the number of lesions or positive correlation with the risk of no new lesion). The arrow heads containing a zero indicate results of the zero-part. Only significant correlations (after FDR-corrections) are shown. We found an autocorrelative behaviour of periventricular, juxtacortical and infratentorial lesions. In the periventricular and juxtacortical region, baseline lesions were significantly associated with new lesions by a positive correlation with the number of new lesions (rate ratio periventricular new lesions, 1.089; p value, < 0.001; rate ratio new juxtacortical lesions, 1.013; p-value < 0.001). For infratentorial lesions, a negative correlation with the risk of no new lesions was observed (odds ratio 0.674; p value, 0.004). In addition, the risk of new periventricular lesions was negatively associated with baseline subcortical lesions (rate ratio, 0.980; p-value, 0.001); the risk of new juxtacortical lesions additionally showed a positive association with the number of baseline periventricular lesions (rate ratio, 1.042; p-value < 0.001) and a negative association with the number of baseline infratentorial lesions (rate ratio, 0.923; p-value 0.006). New subcortical lesions did not show an autocorrelative behaviour; they were positively associated with baseline periventricular lesions (rate ratio, 1.050; p value, < 0.001) and negatively with baseline infratentorial lesions (positive correlation with the risk of no new lesions; rate ratio 0.961; p-value, 0.011).

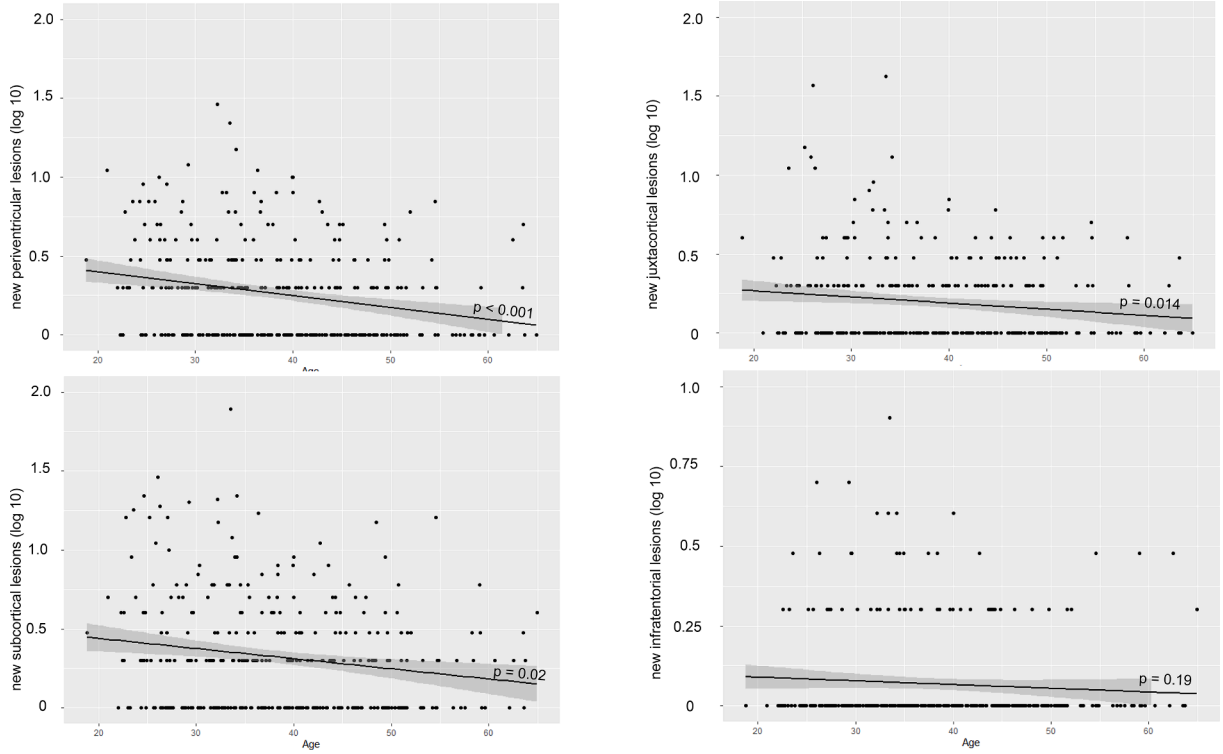

Fig. 4. The association between the number of new lesions in the different locations and age is illustrated by scatter plots. Linear regression line was superimposed in black. The y-axis is noted on a logarithmic scale. To improve visualization, the y-axis was adapted for infratentorial lesions.

Table 4
Parameter estimates zero-inflated Poisson models.

	new PVL		new JCL		new SCL		new ITL	
	Rate Ratio 95 % KI p-value	Odds Ratio 95 % KI p-value	Rate Ratio 95 % KI p-value	Odds Ratio 95 % KI p-value	Rate Ratio 95 % KI p-value	Odds Ratio 95 % KI p-value	Rate Ratio 95 % KI p-value	Odds Ratio 95 % KI p-value
BL PVL	*1.089 1.064; 1.113 < 0.001	0.932 0.871; 0.996 0.039	*1.042 1.017; 1.068 < 0.001	0.934 0.865; 1.009 0.083	*1.050 1.035; 1.065 < 0.001	0.953 0.895; 1.015 0.136	1.041 0.965; 1.122 0.299	0.984 0.871; 1.111 0.791
BL JCL	1.001 0.990; 1.012 0.83	0.969 0.929; 1.012 0.155	*1.013 1.006; 1.021 < 0.001	0.986 0.953; 1.021 0.426	1.006 1.001; 1.011 0.027	0.990 0.949; 1.033 0.638	0.998 0.961; 1.037 0.921	0.928 0.845; 1.018 0.115
BL SCL	**0.980 0.968; 0.992 0.001	1.030 0.997; 1.065 0.079	1.013 1.001; 1.024 0.029	1.015 0.985; 1.047 0.32	1.007 1.000; 1.014 0.051	0.994 0.967; 1.022 0.663	1.009 0.963; 1.058 0.697	1.093 1.007; 1.186 0.034
BL ITL	0.998 0.955; 1.043 0.943	1.022 0.892; 1.172 0.753	**0.923 0.872; 0.977 0.006	0.956 0.808; 1.130 0.596	**0.961 0.932; 0.991 0.011	0.939 0.812; 1.086 0.395	0.953 0.864; 1.051 0.333	*0.674 0.515; 0.882 0.004
age	0.976 0.965; 0.988 < 0.001	1.045 1.015; 1.075 0.003	0.959 0.945; 0.973 < 0.001	0.986 0.950; 1.024 0.474	0.968 0.960; 0.977 < 0.001	1.005 0.978; 1.033 0.706	0.961 0.921; 1.003 0.065	0.959 0.895; 1.028 0.236
gender (male)	0.873 0.699; 1.089 0.229	1.081 0.603; 1.938 0.795	0.705 0.517; 0.963 0.028	1.267 0.640; 2.509 0.497	0.815 0.681; 0.975 0.025	1.493 0.875; 2.547 0.141	1.534 0.789; 2.982 0.207	1.453 0.504; 4.191 0.489

Significant (after FDR-correction) positive correlations of baseline lesions with new lesions (positive correlation with the number of lesions or negative correlation with the risk of no new lesion) are notified with *. Significant (after FDR-correction) negative correlations of baseline lesions with new lesions (negative correlation with the number of lesions or positive correlation with the risk of no new lesion) are notified with **.

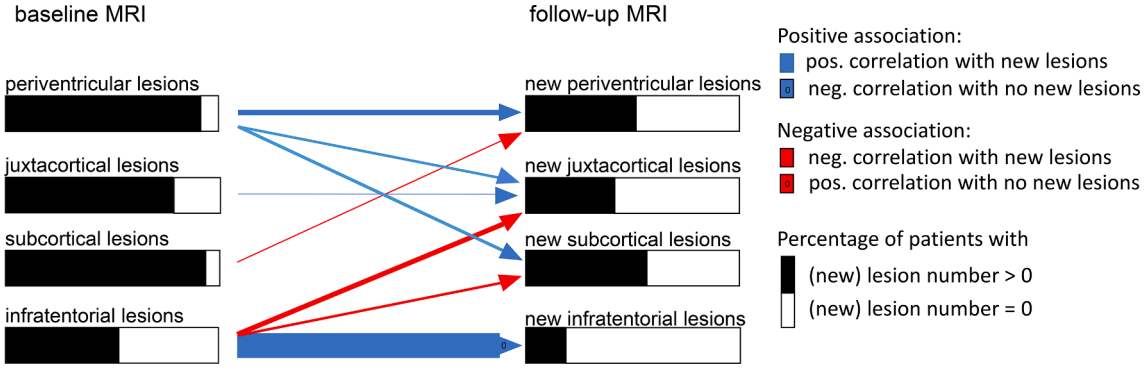

Fig. 5. The results of the zero-inflated Poisson models investigating the association between lesions in the different diagnostic regions at baseline and new lesions at follow-up MRI are illustrated. The blue arrows indicate a positive association between baseline lesions and new solitary lesions (positive correlation with the number of lesions or negative correlation with the risk of no new lesion); red arrows indicate negative associations (negative correlation with the number of lesions or positive correlation with the risk of no new lesion). The arrow heads containing a zero indicate results of the zero-part. Only significant correlations (after FDR-corrections) are shown. (For interpretation of the references to colour in this figure legend, the reader is referred to the web version of this article.)

3.6. Association of baseline and new solitary lesions with EDSS

The cohort was clinically relatively stable and mildly affected. The median EDSS (1.5) did not change between baseline and follow-up MRI. Score on the EDSS was between 0 and 2 in 85 % of the patients at baseline and 86 % of the patients at follow-up (Table 1). The association of baseline and new solitary lesions with EDSS at baseline and follow-up is given in Table 5. Follow-up EDSS correlated with total lesion numbers in all regions but not with the number of new lesions. EDSS at baseline correlated with baseline periventricular lesion volume only.

4. Discussion

In this study of patients with MS, we thoroughly investigated white matter lesions by high-resolution conventional MRI. We demonstrated that, over time, spatial lesion patterns across diagnostic brain regions are not random; instead, there is a significant autocorrelative behavior of periventricular, juxtacortical, and infratentorial lesions. We will discuss our findings with special attention to subcortical lesions.

The distribution of lesion volumes in our study demonstrated the characteristic central to peripheral gradient in the supratentorial brain that had been described before in numerous studies (Altermatt et al., 2018; Di Perri et al., 2008; Giorgio et al., 2020; Giorgio et al., 2013; Lee et al., 1999). In our study, subcortical lesions were found in more than

Table 5
Correlation of lesion numbers with EDSS.

		EDSS BL	EDSS FU
BL PVL	Pearson correlation	0.175	0.215
	significance	0.003	0.000
	N	284	321
BL JCL	Pearson correlation	0.091	0.181
	significance	0.125	0.001
	N	284	321
BL SCL	Pearson correlation	0.119	0.196
	significance	0.045	0.000
	N	284	321
BL ITL	Pearson correlation	0.105	0.160
	significance	0.077	0.004
	N	284	321
new PVL	Pearson correlation	0.041	0.021
	significance	0.496	0.715
	N	283	320
new JCL	Pearson correlation	−0.040	−0.042
	significance	0.507	0.449
	N	283	320
new SCL	Pearson correlation	0.020	0.013
	significance	0.735	0.813
	N	283	320
new ITL	Pearson correlation	0.008	0.024
	significance	0.898	0.673
	N	283	320

Significant (FDR-corrected) positive correlations are highlighted in blue.

90 % of MS patients and substantially contributed to overall lesion burden. We hypothesize that the lower periventricular lesion number compared to subcortical lesions despite the largest lesion volume is due to a higher proportion of confluent lesions in the periventricular region. The high percentage of lesion changes abutting another lesion in the periventricular region (Table 3) supports this hypothesis. The high number of subcortical lesions may be a consequence of the high-resolution and field strength of the sequences used in our study (1x 1x 1.5 mm at 3 Tesla) enabling the assignment of subcortical lesions as such, even in case they are located near the cortical ribbon or close to the ventricles. In contrast, this may not have been possible in the studies (3–5 mm slice thickness at 1.5 Tesla) having substantiated the current diagnostic criteria (Swanton et al., 2007). In our study, subcortical lesions were less likely to show gadolinium enhancement compared to lesions in the diagnostic regions. One possible explanation for this finding is that also in MS patients, some subcortical lesions are caused by accompanying cardiovascular or neurological diseases like migraine or normal ageing (Awad et al., 1986; Geraldes et al., 2018; Hunt et al., 1989; King et al., 2014; Lapucci et al., 2019; Scharf et al., 2019). However, arterial hypertension was present in 30 and diabetes mellitus in 3 of our patients; further, after exclusion of these 33 patients, we observed virtually the same lesion distribution over the 4 investigated areas (data not shown) indicating that these effects were not driven by few cases of overt cardiovascular comorbidity. Along the same line, we found that subcortical lesions less frequently occurred with increasing age as do lesions in the diagnostic regions (Li et al., 2006). Taken together, we believe that in our cohort most subcortical lesions are due to MS. This supports the current handling of subcortical lesions: At the earliest timepoint, when alternative causes come into consideration, subcortical lesions do not contribute to the diagnosis of MS whereas later they are an established marker of disease activity as important as lesions in the diagnostic regions. This seems justified as the a-priori likelihood of a subcortical lesion being caused by MS should considerably increase, once the diagnosis of MS is established. It remains open for study whether dividing the subcortical region into subregions helps to better characterize subcortical lesions with regard to their specificity for MS.

Finally, our study demonstrated that, intraindividually, the location of new solitary lesions is not random, but shows a significant auto-correlative behavior of periventricular, juxtacortical and infratentorial lesions. However, these associations were relatively weak and it seems unlikely that lesion load across these four brain regions alone can serve as a basis for clustering of patient groups to better address the heterogeneity of MS in research or clinical practice.

In summary, our study demonstrated that, when assessed with high resolution at 3 Tesla, subcortical lesions are found in the majority of MS patients and represent the lesion type most often found as new solitary lesion in follow-up brain MRI scans. Across diagnostic regions, brain white matter lesion formation does not occur in a spatially random manner.

Declaration of Competing Interest

The authors declare that they have no known competing financial interests or personal relationships that could have appeared to influence the work reported in this paper.

Data availability

Data will be made available on request.

Acknowledgements

Viola Pongratz received research support from NOVARTIS Pharma GmbH, Germany (Oppenheim Förderpreis 2017). Benedikt Wiestler und Mark Mühlau received research support from the German Research Foundation (DFG SPP2177, Radiomics: Next Generation of Biomedical Imaging – project number 428223038). This study was also supported by the DIFUTURE consortium (Data Integration for Future Medicine), funded by the German Federal Ministry of Education and Research (BMBF) within the Medical Informatics Initiative (grants 01ZZ1603[A-D] and 01ZZ1804[A-I]). Christiane Gasperi reports funding from the German Research Foundation (Deutsche Forschungsgesellschaft DFG), the Hertie Foundation, the Hans and Klementia Langmatz, and the German Federal Ministry of Education and Research, all of which are not related to this study. Bernhard Hemmer received research support from the EU Project MultipleMS and the Deutsche Forschungsgemeinschaft (DFG, German Research Foundation) under Germany's Excellence Strategy within the framework of the Munich Cluster for Systems Neurology [EXC 2145 SyNergy – ID 390857198].

Disclosures

Viola Pongratz received research support from NOVARTIS Pharma GmbH, Germany (Oppenheim Förderpreis 2017).

Christiane Gasperi Christiane Gasperi reports funding from the German Research Foundation (Deutsche Forschungsgesellschaft DFG), the Hertie Foundation, the Hans and Klementia Langmatz, and the German Federal Ministry of Education and Research, all of which are not related to this study.

Benedikt Wiestler has received speaker honoraria from Philips and research support from the German Research Foundation (DFG SPP2177, Radiomics: Next Generation of Biomedical Imaging – project number 428223038).

Jan Kirschke has received research funding from the German Research Foundation (Deutsche Forschungsgemeinschaft, DFG; project 432290010), the German Federal Ministry of Education and Research (13GW0469D) and the European Research Council (ERC) under the

European Union's Horizon 2020 research and innovation programme (101045128 — iBack-epic — ERC-2021-COG). He is Co-Founder of Bonescreen GmbH.

Klaus Zimmer has nothing to disclose.

Achim Berthele has received consulting and/or speaker fees from Alexion, Bayer Healthcare, Biogen, Celgene, Novartis, Roche and Sandoz/Hexal. His institution has received compensation for clinical trials from Alexion, Biogen, Merck, Novartis, Roche, and Sanofi Genzyme. Bernhard Hemmer is associated with DIFUTURE (Data Integration for Future Medicine) [BMBF 01ZZ1804[A-I]].

Bernhard Hemmer has received research support from the EU Project MultipleMS and the Deutsche Forschungsgemeinschaft (DFG, German Research Foundation) under Germany's Excellence Strategy within the framework of the Munich Cluster for Systems Neurology [EXC 2145 SyNergy – ID 390857198].

Mark Mühlau has received research support from the Bavarian State Ministry for Science and Art (Collaborative Bilateral Research Program Bavaria – Québec: AI in medicine, grant F.4-V0134.K5.1/86/34), the German Research Foundation (DFG SPP2177; Radiomics: Next Generation of Biomedical Imaging; project number 428223038); the National Institutes of Health (grant 1R01NS112161-01); the German Federal Ministry of Education and Research (DIFUTURE: 01ZZ1603[A-D] and 01ZZ1804[A-I]).

Subcortical lesions are found in the majority of patients with Multiple sclerosis.

Brain white matter lesion formation follows individual spatial patterns.

References

Absinta, M., Sati, P., Reich, D.S., 2016. Advanced MRI and staging of multiple sclerosis lesions. Nat Rev Neurol 12, 358–368.

Altermatt, A., Gaetano, L., Magon, S., Häring, D.A., Tomic, D., Wuerfel, J., Radue, E.W., Kappos, L., Sprenger, T., 2018. Clinical Correlations of Brain Lesion Location in Multiple Sclerosis: Voxel-Based Analysis of a Large Clinical Trial Dataset. Brain Topogr 31, 886–894.

Awad, I.A., Spetzler, R.F., Hodak, J.A., Awad, C.A., Carey, R., 1986. Incidental subcortical lesions identified on magnetic resonance imaging in the elderly. I. Correlation with age and cerebrovascular risk factors. Stroke 17, 1084–1089.

Benjamini, Y., Hochberg, Y., 1995. Controlling the False Discovery Rate: A Practical and Powerful Approach to Multiple Testing. Journal of the Royal Statistical Society. Series B (Methodological) 57, 289–300.

Cohen, J.A., Arnold, D.L., Comi, G., Bar-Or, A., Gujrathi, S., Hartung, J.P., Cravets, M., Olson, A., Frohna, P.A., Selmaj, K.W., 2016. Safety and efficacy of the selective sphingosine 1-phosphate receptor modulator ozanimod in relapsing multiple sclerosis (RADIANCE): a randomised, placebo-controlled, phase 2 trial. Lancet Neurol 15, 373–381.

Cohen, J.A., Coles, A.J., Arnold, D.L., Confavreux, C., Fox, E.J., Hartung, H.P., Havrdova, E., Selmaj, K.W., Weiner, H.L., Fisher, E., Brinar, V.V., Giovannoni, G., Stojanovic, M., Ertik, B.I., Lake, S.L., Margolin, D.H., Panzara, M.A., Compston, D.A., 2012. Alemtuzumab versus interferon beta 1a as first-line treatment for patients with relapsing-remitting multiple sclerosis: a randomised controlled phase 3 trial. Lancet.

Coles, A.J., Twyman, C.L., Arnold, D.L., Cohen, J.A., Confavreux, C., Fox, E.J., Hartung, H.P., Havrdova, E., Selmaj, K.W., Weiner, H.L., Miller, T., Fisher, E., Sandbrink, R., Lake, S.L., Margolin, D.H., Oyuela, P., Panzara, M.A., Compston, D.A., 2012. Alemtuzumab for patients with relapsing multiple sclerosis after disease-modifying therapy: a randomised controlled phase 3 trial. Lancet.

Comi, G., Filippi, M., Barkhof, F., Durelli, L., Edan, G., Fernandez, O., Hartung, H., Seeldrayers, P., Sorensen, P.S., Rovaris, M., Martinelli, V., Hommes, O.R., 2001. Effect of early interferon treatment on conversion to definite multiple sclerosis: a randomised study. Lancet 357, 1576–1582.

Comi, G., Martinelli, V., Rodegher, M., Moiola, L., Bajenaru, O., Carra, A., Elovaara, I., Fazekas, F., Hartung, H.P., Hillert, J., King, J., Komoly, S., Lubetzki, C., Montalban, X., Myhr, K.M., Ravnborg, M., Rieckmann, P., Wynn, D., Young, C., Filippi, M., 2009. Effect of glatiramer acetate on conversion to clinically definite multiple sclerosis in patients with clinically isolated syndrome (PreCISe study): a randomised, double-blind, placebo-controlled trial. Lancet 374, 1503–1511.

Di Perri, C., Battaglini, M., Stromillo, M.L., Bartolozzi, M.L., Guidi, L., Federico, A., De Stefano, N., 2008. Voxel-based assessment of differences in damage and distribution of white matter lesions between patients with primary progressive and relapsing-remitting multiple sclerosis. Arch Neurol 65, 236–243.

Eichinger, P., Wiestler, H., Zhang, H., Biberacher, V., Kirschke, J.S., Zimmer, C., Mühlau, M., Wiestler, B., 2017. A novel imaging technique for better detecting new lesions in multiple sclerosis. J Neurol 264, 1909–1918.

Ebers, G.C., 1998. Randomised double-blind placebo-controlled study of interferon beta-1a in relapsing/remitting multiple sclerosis. PRISMS (Prevention of Relapses and Disability by Interferon beta-1a Subcutaneously in Multiple Sclerosis) Study Group. Lancet 352, 1498–1504.

Eichinger, P., Schön, S., Pongratz, V., Wiestler, H., Zhang, H., Bussas, M., Hoshi, M.M., Kirschke, J., Berthele, A., Zimmer, C., Hemmer, B., Mühlau, M., Wiestler, B., 2019. Accuracy of Unenhanced MRI in the Detection of New Brain Lesions in Multiple Sclerosis. Radiology 291, 429–435.

Fox, R.J., Miller, D.H., Phillips, J.T., Hutchinson, M., Havrdova, E., Kita, M., Yang, M., Raghupathi, K., Novas, M., Sweetser, M.T., Viglietta, V., Dawson, K.T., 2012. Placebo-controlled phase 3 study of oral BG-12 or glatiramer in multiple sclerosis. N Engl J Med 367, 1087–1097.

Gaetano, L., Magnusson, B., Kindalova, P., Tomic, D., Silva, D., Altermatt, A., Magon, S., Müller-Lenke, N., Radue, E.W., Leppert, D., Kappos, L., Wuerfel, J., Häring, D.A., Sprenger, T., 2020. White matter lesion location correlates with disability in relapsing multiple sclerosis. Mult Scler J Exp Transl Clin 6, 2055.

Geraldes, R., Ciccarelli, O., Barkhof, F., De Stefano, N., Enzinger, C., Filippi, M., Hofer, M., Paul, F., Preziosa, P., Rovira, A., DeLuca, G.C., Kappos, L., Yousry, T., Fazekas, F., Frederiksen, J., Gasperini, C., Sastre-Garriga, J., Evangelou, N., Palace, J., on behalf of the, M.s.g., 2018. The current role of MRI in differentiating multiple sclerosis from its imaging mimics. Nature Reviews Neurology 14, 199-213.

Giorgio, A., Battaglini, M., Rocca, M.A., De Leucio, A., Absinta, M., van Schijndel, R., Rovira, A., Tintoré, M., Chard, D., Ciccarelli, O., Enzinger, C., Gasperini, C., Frederiksen, J., Filippi, M., Barkhof, F., De Stefano, N., 2013. Location of brain lesions predicts conversion of clinically isolated syndromes to multiple sclerosis. Neurology 80, 234–241.

Giorgio, A., Battaglini, M., Gentile, G., Stromillo, M.L., Gasperini, C., Visconti, A., Paolillo, A., De Stefano, N., 2020. Mapping the Progressive Treatment-Related Reduction of Active MRI Lesions in Multiple Sclerosis. Front Neurol 11, 585296.

Giovannoni, G., Comi, G., Cook, S., Rammohan, K., Rieckmann, P., Soelberg Sorensen, P., Vermersch, P., Chang, P., Hamlett, A., Musch, B., Greenberg, S.J., 2010. A placebo-controlled trial of oral cladribine for relapsing multiple sclerosis. N Engl J Med 362, 416–426.

Gold, R., Kappos, L., Arnold, D.L., Bar-Or, A., Giovannoni, G., Selmaj, K., Tornatore, C., Sweetser, M.T., Yang, M., Sheikh, S.I., Dawson, K.T., 2012. Placebo-controlled phase 3 study of oral BG-12 for relapsing multiple sclerosis. N Engl J Med 367, 1098–1107.

Hauser, S.L., Bar-Or, A., Cohen, J.A., Comi, G., Correale, J., Coyle, P.K., Cross, A.H., de Seze, J., Leppert, D., Montalban, X., Selmaj, K., Wiendl, H., Kerloeguen, C., Willi, R., Li, B., Kakarieka, A., Tomic, D., Goodyear, A., Pingili, R., Häring, D.A., Ramanathan, K., Merschhemke, M., Kappos, L., 2020. Ofatumumab versus Teriflunomide in Multiple Sclerosis. N Engl J Med 383, 546–557.

Hauser, S.L., Bar-Or, A., Comi, G., Giovannoni, G., Hartung, H.P., Hemmer, B., Lublin, F., Montalban, X., Rammohan, K.W., Selmaj, K., Traboulsee, A., Wolinsky, J.S., Arnold, D.L., Klingelschmitt, G., Masterman, D., Fontoura, P., Belachew, S., Chin, P., Mairon, N., Garren, H., Kappos, L., 2017. Ocrelizumab versus Interferon Beta-1a in Relapsing Multiple Sclerosis. N Engl J Med 376, 221–234.

Hunt, A.L., Orrison, W.W., Yeo, R.A., Haaland, K.Y., Rhyne, R.L., Garry, P.J., Rosenberg, G.A., 1989. Clinical significance of MRI white matter lesions in the elderly. Neurology 39, 1470–1474.

Kappos, L., 1998. Placebo-controlled multicentre randomised trial of interferon beta-1b in treatment of secondary progressive multiple sclerosis. European Study Group on interferon beta-1b in secondary progressive MS. Lancet 352, 1491–1497.

Kappos, L., Bar-Or, A., Cree, B.A.C., Fox, R.J., Giovannoni, G., Gold, R., Vermersch, P., Arnold, D.L., Arnould, S., Scherz, T., Wolf, C., Wallström, E., Dahlke, F., 2018. Siponimod versus placebo in secondary progressive multiple sclerosis (EXPAND): a double-blind, randomised, phase 3 study. Lancet 391, 1263–1273.

Kappos, L., Fox, R.J., Burcklen, M., Freedman, M.S., Havrdová, E.K., Hennessy, B., Hohlfeld, R., Lublin, F., Montalban, X., Pozzilli, C., Scherz, T., D'Ambrosio, D., Linscheid, P., Vaclavkova, A., Pirozek-Lawniczek, M., Kracker, H., Sprenger, T., 2021. Ponesimod Compared With Teriflunomide in Patients With Relapsing Multiple Sclerosis in the Active-Comparator Phase 3 OPTIMUM Study: A Randomized Clinical Trial. Jama Neurology 78, 558–567.

Kappos, L., Radue, E.W., O'Connor, P., Polman, C., Hohlfeld, R., Calabresi, P., Selmaj, K., Agoropoulou, C., Leyk, M., Zhang-Auberson, L., Burtin, P., 2010. A placebo-controlled trial of oral fingolimod in relapsing multiple sclerosis. N Engl J Med 362, 387–401.

Khatri, B., Barkhof, F., Comi, G., Hartung, H.P., Kappos, L., Montalban, X., Pelletier, J., Stites, T., Wu, S., Holdbrook, F., Zhang-Auberson, L., Francis, G., Cohen, J.A., 2011. Comparison of fingolimod with interferon beta-1a in relapsing-remitting multiple sclerosis: a randomised extension of the TRANSFORMS study. Lancet Neurol 10, 520–529.

King, K.S., Peshock, R.M., Rossetti, H.C., McColl, R.W., Ayers, C.R., Hulsey, K.M., Das, S. R., 2014. Effect of normal aging versus hypertension, abnormal body mass index, and diabetes mellitus on white matter hyperintensity volume. Stroke 45, 255–257.

Lapucci, C., Saitta, L., Bommarito, G., Sormani, M.P., Pardini, M., Bonzano, L., Mancardi, G.L., Gasperini, C., Giorgio, A., Inglese, M., De Stefano, N., Roccatagliata, L., 2019. How much do periventricular lesions assist in distinguishing migraine with aura from CIS? Neurology 92, e1739 e1744.

Lee, M.A., Smith, S., Palace, J., Narayanan, S., Silver, N., Minicucci, L., Filippi, M., Miller, D.H., Arnold, D.L., Matthews, P.M., 1999. Spatial mapping of T2 and gadolinium-enhancing T1 lesion volumes in multiple sclerosis: evidence for distinct mechanisms of lesion genesis? Brain 122 (Pt 7), 1261–1270.

Leist, T.P., Comi, G., Cree, B.A., Coyle, P.K., Freedman, M.S., Hartung, H.P., Vermersch, P., Casset-Semanaz, F., Scaramozza, M., 2014. Effect of oral cladribine on time to conversion to clinically definite multiple sclerosis in patients with a first demyelinating event (ORACLE MS): a phase 3 randomised trial. Lancet Neurol.

Li, D.K., Held, U., Petkau, J., Daumer, M., Barkhof, F., Fazekas, F., Frank, J.A., Kappos, L., Miller, D.H., Simon, J.H., Wolinsky, J.S., Filippi, M., 2006. MRI T2 lesion

burden in multiple sclerosis: a plateauing relationship with clinical disability. Neurology 66, 1384–1389.
McDonald, W.I., Compston, A., Edan, G., Goodkin, D., Hartung, H.P., Lublin, F.D., McFarland, H.F., Paty, D.W., Polman, C.H., Reingold, S.C., Sandberg-Wollheim, M., Sibley, W., Thompson, A., van den Noort, S., Weinshenker, B.Y., Wolinsky, J.S., 2001. Recommended diagnostic criteria for multiple sclerosis: guidelines from the International Panel on the diagnosis of multiple sclerosis. Ann Neurol 50, 121–127.
Montalban, X., Hauser, S.L., Kappos, L., Arnold, D.L., Bar-Or, A., Comi, G., de Seze, J., Giovannoni, G., Hartung, H.-P., Hemmer, B., Lublin, F., Rammohan, K.W., Selmaj, K., Traboulsee, A., Sauter, A., Masterman, D., Fontoura, P., Belachew, S., Garren, H., Mairon, N., Chin, P., Wolinsky, J.S., 2016. Ocrelizumab versus Placebo in Primary Progressive Multiple Sclerosis. New England Journal of Medicine 376, 209–220.
Polman, C.H., O'Connor, P.W., Havrdova, E., Hutchinson, M., Kappos, L., Miller, D.H., Phillips, J.T., Lublin, F.D., Giovannoni, G., Wajgt, A., Toal, M., Lynn, F., Panzara, M. A., Sandrock, A.W., 2006. A randomized, placebo-controlled trial of natalizumab for relapsing multiple sclerosis. N Engl J Med 354, 899–910.
Scharf, E.L., Graff-Radford, J., Przybelski, S.A., Lesnick, T.G., Mielke, M.M., Knopman, D. S., Preboske, G.M., Schwarz, C.G., Senjem, M.L., Gunter, J.L., Machulda, M., Kantarci, K., Petersen, R.C., Jack Jr., C.R., Vemuri, P., 2019. Cardiometabolic Health and Longitudinal Progression of White Matter Hyperintensity: The Mayo Clinic Study of Aging. Stroke 50, 3037–3044.
Swanton, J.K., Rovira, A., Tintore, M., Altmann, D.R., Barkhof, F., Filippi, M., Huerga, E., Miszkiel, K.A., Plant, G.T., Polman, C., Rovaris, M., Thompson, A.J., Montalban, X., Miller, D.H., 2007. MRI criteria for multiple sclerosis in patients presenting with clinically isolated syndromes: a multicentre retrospective study. Lancet Neurol 6, 677–686.
Tallantyre, E.C., Brookes, M.J., Dixon, J.E., Morgan, P.S., Evangelou, N., Morris, P.G., 2008. Demonstrating the perivascular distribution of MS lesions in vivo with 7-Tesla MRI. Neurology 70, 2076–2078.
Thompson, A.J., Banwell, B.L., Barkhof, F., Carroll, W.M., Coetzee, T., Comi, G., Correale, J., Fazekas, F., Filippi, M., Freedman, M.S., Fujihara, K., Galetta, S.L., Hartung, H.P., Kappos, L., Lublin, F.D., Marrie, R.A., Miller, A.E., Miller, D.H., Montalban, X., Mowry, E.M., Sorensen, P.S., Tintoré, M., Traboulsee, A.L., Trojano, M., Uitdehaag, B.M.J., Vukusic, S., Waubant, E., Weinshenker, B.G., Reingold, S.C., Cohen, J.A., 2018. Diagnosis of multiple sclerosis: 2017 revisions of the McDonald criteria. The Lancet Neurology 17, 162–173.
Yushkevich, P.A., Piven, J., Hazlett, H.C., Smith, R.G., Ho, S., Gee, J.C., Gerig, G., 2006. User-guided 3D active contour segmentation of anatomical structures: significantly improved efficiency and reliability. Neuroimage 31, 1116–1128.